

On the Relation Between Storm Tracks and North American Precipitation in  
the Boreal Winter

Katherine E. Lukens

A scholarly paper in partial fulfillment of the requirements for the degree of  
Master of Science

April 2015

Department of Atmospheric and Oceanic Science, University of Maryland  
College Park, Maryland

Advisor: Dr. Ernesto Hugo Berbery

## Table of Contents

<b>Abstract.....</b>	<b>ii</b>
<b>Acknowledgements.....</b>	<b>iii</b>
List of Figures.....	iv
List of Symbols.....	v
<b>Chapter 1. Introduction.....</b>	<b>1</b>
<b>Chapter 2. Methods.....</b>	<b>9</b>
2.1 Eulerian Approach.....	9
2.2 Lagrangian Approach.....	10
<b>Chapter 3. Results.....</b>	<b>12</b>
3.1 Eulerian Approach.....	12
3.2 Lagrangian Approach.....	17
3.2.1 Pacific Storm Track.....	22
3.2.2 North American-Atlantic Storm Track.....	24
3.2.3 Mediterranean Storm Track and Other Features.....	26
<b>Chapter 4. Discussion.....</b>	<b>29</b>
4.1 Comparisons between variables using Eulerian Approach.....	29
4.2 Comparisons between Eulerian and Lagrangian Approaches.....	29
4.2.1 Pacific Storm Track.....	30
4.2.2 North American-Atlantic Storm Track.....	31
4.2.3 Mediterranean Storm Track.....	32
4.3 Lagrangian comparisons between $\zeta_{850}$ and $PV_{320}$ .....	33
4.3.1 Pacific Storm Track.....	33
4.3.2 North America-Atlantic Storm Track.....	34
4.3.3 Mediterranean Storm Track.....	35
<b>Chapter 5. Conclusions.....</b>	<b>36</b>
<b>References.....</b>	<b>38</b>

## Abstract

Groups of storms, known as storm tracks, can have a profound impact on the climate by influencing the variability in cyclonic activity in the mid-latitudes. This study investigates the behaviors of Northern Hemisphere winter storm tracks and their relation to surface precipitation in North America. A local diagnostic and a cyclone tracking algorithm are used to quantify storm tracks described by 200hPa winds, 850hPa vorticity, and potential vorticity at  $\theta=320\text{K}$  from NCEP's Climate Forecast System Reanalysis (CFSR) product. Statistics are computed using these variables, revealing detailed characteristics of storm tracks. Isentropic potential vorticity within the Lagrangian framework is determined to be the preferred combination of variable and methodology to describe storm tracks. This combination reveals three distinct storm tracks, as well as regions of cyclogenesis and cyclolysis. The precipitation associated with identified cyclones is computed. Storm tracks identified from isentropic potential vorticity leave a strong footprint in surface precipitation, exposing small scaled features of precipitation patterns in North America.

## **Acknowledgements**

The author thanks Dr. E. Hugo Berbery for his patient and indispensable advice of this work. The author also thanks Dr. Kevin I. Hodges for providing essential computational support for the feature tracking program.

## List of Figures

<u>Figure</u>	<u>Page</u>
1. Mean of u at 200mb for DJF 1980-2010, non-polar, global.....	12
2A. Standard deviation of v at 200mb for DJF 1980-2010, polar, NH.....	13
2B. Standard deviation of v at 200mb for DJF 1980-2010, global.....	13
2C. Standard deviation of v at 200mb for DJF 1980-2010, North America.....	13
3A. One-point Correlations of v at 200hPa for DJF 1979-2010, North America.....	14
3B. One-point Correlations of v at 200hPa on precip for DJF 1979-2010, North America.....	15
4. Standard deviation of vorticity at 850mb for DJF 1980-2010, polar, NH.....	16
5A. Regression of vorticity at 850hPa for DJF 1979-2010, global.....	16
5B. Regression of vorticity on precip at 850hPa for DJF 1979-2010, global.....	16
6A. 1980 DJF vorticity at 850hPa trajectories, North America.....	18
6B. 1980 DJF potential vorticity at 320K trajectories, North America.....	18
6C. 1980-2010 DJF potential vorticity at 320K trajectories, polar, NH.....	18
7A. 1980-2010 DJF vorticity at 850hPa Track Density, polar, NH.....	19
7B. 1980-2010 DJF potential vorticity at 320K Track Density, polar, NH.....	19
8A. 1980-2010 DJF vorticity at 850hPa Mean Intensity, polar, NH.....	19
8B. 1980-2010 DJF potential vorticity at 320K Mean Intensity, polar, NH.....	19
9A. 1980-2010 DJF vorticity at 850hPa Genesis Density, polar, NH.....	21
9B. 1980-2010 DJF potential vorticity at 320K Genesis Density, polar, NH.....	21
10A. 1980-2010 DJF vorticity at 850hPa Lysis Density, polar, NH.....	21
10B. 1980-2010 DJF potential vorticity at 320K Lysis Density, polar, NH.....	21
11A. 1980-2010 DJF Mean Intensity of precip associated with vorticity at 850hPa, polar, NH.....	22
11B. 1980-2010 DJF Mean Intensity of precip associated with potential vorticity at 320K, polar, NH.....	22

## List of Symbols

- A.  $\zeta_{850}$  – vorticity at 850hPa following the Lagrangian framework
- B.  $\theta$  – vertical level in units of Kelvin (K)
- C.  $PV_{320}$  – potential vorticity on an isentropic surface of  $\theta=320\text{K}$

## Chapter 1. Introduction

While storms strongly influence local weather, groups of storms can impact the climate by contributing to shifts in tropospheric jets, and altering global atmospheric flow patterns. Wallace et al. (1988) explored the influences of both cyclones and anticyclones on regions of high variability in the Northern Hemisphere. They deduced that cyclones follow the baroclinic waveguides and move northeastward (In the Northern Hemisphere) towards climatological oceanic low pressure systems; anticyclones follow the same waveguides and move southeastward towards climatological oceanic high pressure systems. They defined these regions as baroclinic waveguides or areas of strong variability that coincide with bands of strong teleconnectivity, which quantifies “the extent to which high-frequency fluctuations are wavelike.” They described the evolution of baroclinic waves as exerting westerly flows that contribute to the surface winds, causing cyclones (anticyclones) at the surface to drift poleward (equatorward) relative to the background flow. Chang and Orlanski (1993) also found that the temporal evolution of this large-scale eddy activity remained confined to certain latitude bands. These spatial bands of large-scale eddy development are paths along which cyclones and anticyclones most likely travel, and so they can be thought of as baroclinic waveguides, or storm tracks.

Many studies on baroclinic wave activity have only considered cyclones when investigating storm track patterns and characteristics during their analyses. The term “storm track” can thus be misleading, for it implies that cyclones solely follow these paths while ignoring the development and propagation of anticyclones.

Hoskins and Valdes (1990) supplemented this description through the examination of vorticity fluxes, demonstrating that divergence aloft produces a cyclonic (anticyclonic) circulation poleward (equatorward) of the large-scale eddy activity, generating upstream confluence. If this confluence is strong enough, it can predominantly contribute to the maintenance of the mean baroclinicity needed to sustain baroclinic waves downstream. The growth and decay of individual storms is influenced by surface friction, orographic effects, and the state of the atmosphere at the time of the storm's initial development.

While baroclinicity is a key ingredient of the storm tracks, Orlanski and Chang (1993) found that ageostrophic fluxes radiated by upstream eddies trigger the development and maintenance of new eddies downstream, despite the lower baroclinicity there. Unstable upstream eddies then decay due to the radiation of energy downstream; the more stable downstream eddies grow from this influx of energy and decay from the subsequent divergence of ageostrophic geopotential fluxes. Individual eddies tend to develop in groups with subsequent eddies developing downstream due to the downstream radiation of energy previously mentioned. These groups of eddies propagate as a large-scale wave packet, moving at a group velocity. The group velocity as described by Orlanski and Chang (1993) primarily dictates the speed at which a wave packet spreads up- and downstream.

Conventional diagnostic methods have provided information regarding general storm track behavior. The extent of storm tracks can be hindered by regions of increased surface roughness and orography. Areas of stronger friction also dissipate the intensity of the storm tracks, allowing for the existence of more localized maxima and minima of

storm track strength (Chang and Orlanski 1993). Storm tracks can be identified as areas of high variability of key variables when studying transient eddies.

Brayshaw et al. (2008) found that the atmospheric baroclinicity along with the relative positions of the subtropical and subpolar jets affect the latitudinal locations of storm tracks. From the previous studies of Hsu and Lin (1992) and Hoskins and Ambrizzi (1993), Lu et al. (2002) interpreted that anomalies of upper tropospheric stream function and vorticity become zonally elongated largely due to the latitudinal shifts in the jet stream brought on by its seasonal and interannual variabilities, making the zonally-oriented Rossby waves associated with these variables unidentifiable. Thus, the stream function and vorticity in the upper troposphere do not well represent storm tracks. Lu et al. (2002) found that zonal Rossby waves associated with the meridional component of the upper tropospheric wind are not noticeably elongated by the jet stream, implying that the meridional wind field better depicts zonally-propagating atmospheric wave patterns. Orlanski and Chang (1993) confirmed the advantage of using this variable during their analyses of the development of individual cyclones: the downstream divergence of the ageostrophic geopotential flux dominates the decay of a cyclone while providing energy for the development of another cyclone farther downstream. Therefore, the analysis of this variable has become standard when studying storm track behavior.

Two well-documented storm tracks in the Northern Hemisphere are the Pacific and Atlantic tracks. These tracks are characterized as zonally elongated regions of high baroclinicity, or deep baroclinic instability. Hoskins and Valdes (1990) found that during the boreal winter, diabatic heating off the western boundaries of Asia and North America act to maintain regions of high atmospheric baroclinicity, making these regions favorable

for increased large-scale eddy activity. They found that both the Atlantic and Pacific storm tracks are well-defined when examining the baroclinicity parameter, or the Eady growth rate maximum; from this view the Atlantic track primarily extends from the eastern coast of North America to northwestern Europe, and the Pacific track primarily extends from the eastern coast of Asia to northwestern North America. The baroclinicity parameter provides a definitive western boundary to both tracks in the form of minimum values downstream of the respective maximums. The standard deviation of the meridional wind at 200 hPa spatially represents the Northern Hemisphere storm track patterns in the DJF season with relative accuracy as it captures the Pacific and Atlantic tracks. The lower atmospheric vorticity field converted is also considered in this local approach; areas of high variability of the 850 hPa vorticity indicate storm track maxima, or areas of strong storm development.

Storm tracks in the Southern Hemisphere differ from their Northern Hemisphere counterparts, primarily due to the greater zonal symmetry in the Southern Hemisphere. Trenberth (1991) suggested that the zonal nature of and the dominant presence of oceans in the Southern Hemisphere allow storm tracks to sustain strong baroclinic activity in both the summer and winter seasons. The strong meridional temperature gradient in the summer season and the prominent maximum in the variance of geopotential height in the southern Indian Ocean in both the summer and winter contribute to the year-round baroclinic wave activity. These waves unceasingly undergo life cycles of growth and decay. Berbery and Vera (1996) documented the behavior of these two storm tracks. In both the subtropical and subpolar storm tracks the well-defined wave packet structures demonstrate that down-stream development contributes to the evolution of the synoptic-scale

waves. The subtropical storm track exhibits a stronger wave packet structure, probably due to its weaker baroclinicity. They also note that, overall, the wave trains produced follow the paths of the subtropical and subpolar jets, with periods and wavelengths similar to those found in the Northern Hemisphere by Wallace et al. (1988), Chang and Orlanski (1993), and others.

Most of the previous studies followed an Eulerian (or local) approach. A more recent method for diagnosing storm tracks is inspired by the Lagrangian view. The Lagrangian view follows an entity throughout its life cycle, contrasting the Eulerian view which observes an entity as it passes over a fixed location. Motivated by the Lagrangian view, Hoskins and Hodges (2002) used feature tracking software to identify 850hPa vorticity maxima as individual cyclones and then track them; they also explored the use of isentropic potential vorticity at 330K to identify and track cyclones. Isentropic potential vorticity (IPV) is conserved for adiabatic, frictionless flow. It is said to “induce” changes in the wind and temperature fields, and so one may conclude that IPV determines the flow field and is advected by it. Because a parcel (i.e., a cyclone) conserves potential vorticity on an isentropic surface, it must move parallel to isocontours of potential vorticity, making this variable ideal for clearly identifying and tracking storms (Holton 2004). Hoskins and Hodges (2002) stressed that the vorticity at 850hPa is the preferred variable to diagnose storm track behavior, explaining that it is able to identify low pressure systems earlier in their life cycles because it is less influenced by the background flow and so it able to better expose smaller spatial scales. This allows for the detection of storm genesis regions, which are typically small in scale. This method allows for the separate extraction and analysis of cyclones and anticyclones, whereas the local diagnostic described above

does not. It also shows better defined and detailed Northern Hemisphere winter storm tracks than the traditional Eulerian method.

The passages of extratropical cyclones are associated with precipitation events. By considering the Lagrangian view, Hawcroft et al. (2012) identified areas within the oceanic regions of the Atlantic and Pacific storm tracks as having the greatest absolute storm associated precipitation, with over 70% of the total precipitation associated with the passage of a cyclone in North America and parts of Europe; they did note that precipitation may be enhanced over mountainous regions due to orographic effects. They also found that heavy precipitating storms have a greater impact on the total precipitation climatology in the DJF season compared to the other seasons because the largest amount of precipitation occurs in the boreal winter.

Studies of daily precipitation characteristics have revealed the importance of relationships between storm tracks, precipitation, and global atmospheric patterns, such as the El Niño Southern Oscillation (ENSO), the Pacific-North American pattern (PNA), and the Madden-Julian Oscillation (MJO). Trenberth et al. (2003) analyzed the various aspects that potentially modulate the characterization of precipitation over time. Storm track changes over the Northern Pacific Ocean associated with the PNA and the positive phase of ENSO create precipitation anomalies that extend south to California and to the southeastern United States, demonstrating increased storm activity and rainfall to the south and decreased rainfall to the north. Salathé (2006) studied the influences of the Aleutian Low on North American precipitation through storm track changes. The location and intensity of this low contributes to the movement and intensification of the storm track in the North Pacific. He also found that a northward shift and deepening of the

Aleutian Low causes a similar shift in the North Pacific storm track, which in turn amplifies winter precipitation and contributes to its northward movement in this area. Becker et al. (2009) examined precipitation characteristics associated with ENSO over the contiguous United States. During winter, they found a 40-60% increase in daily precipitation intensity, defined as a daily average over days with recorded precipitation matching and/or exceeding 1.0 mm, over the southwestern and central United States during an El Niño as compared to a La Niña. Becker et al. (2011) examined these characteristics in conjunction the MJO, focusing on phases 5-7. They found that the frequency of precipitation events, defined as the number of days with recorded precipitation of 1.0 mm or higher, slightly decreased in the Mississippi River basin while substantially dropping in Florida. They also found that the daily precipitation intensity increased in much of the lower Mississippi River basin, implying the development of more intense storms. Precipitation variability and the varying extremes of drastic precipitation events, some of which can last for multiple seasons or years, significantly impact agriculture, businesses, and the general population in North America.

As storms develop and propagate, they affect the environment around them. The goal of this work is to establish a better understanding of the relationship between North American precipitation and the intensities and spatial patterns of storm tracks in the boreal winter. We first apply the Eulerian diagnostic to the meridional wind at 200hPa. We then apply the Lagrangian approach to vorticity at 850hPa and potential vorticity at  $\theta=320\text{K}$  to obtain storm track patterns and extract the surface precipitation associated with each cyclone identified from these patterns. By analyzing these groups of storms of varying se-

verity, we deepen our understanding of how storm track characteristics influence precipitation.

Section II defines the data and methodology used. Section III describes the figures and results produced from this study. Section IV highlights the similarities and differences between the approaches and variables used in our analyses. Section V summarizes our findings detailed in sections III and IV.

## Chapter 2. Methods

The vorticity at 850hPa ( $\zeta_{850}$ ), isentropic potential vorticity at 320K ( $PV_{320}$ ), and precipitation data range from December 1979 to December 2010 and are from the NCEP Climate Forecast System Reanalysis (CFSR) product at a horizontal resolution of 32km. In our analyses we employ the wind components at 200hPa and 850hPa in units of  $m\ s^{-1}$ , the potential vorticity at  $\theta=320K$  in units of one PVU, and the surface precipitation rate in units of  $mm\ day^{-1}$ .

In October 1998, data from the Advance TIROS operational vertical sounder (ATOVS) from the NOAA 15 satellite was assimilated into CFSR. Chelliah et al. (2011) explains that this may be a contributing factor to an observed artificial jump in the precipitation and wind data around this time. For low-level zonal winds, they determined that CFSR data after 1998 agrees with reanalyses from other products for the same time period with no notable systematic differences, while prior to 1998 CFSR demonstrates that equatorial Pacific easterlies are more easterly and equatorial Indian westerlies are more westerly than the other reanalyses. Other reanalysis investigations such as Wang et al. (2011) have found that CFSR provides a better-quality dataset of precipitation than past NCEP reanalyses.

### 2.1 Eulerian Approach

The traditional Eulerian diagnostic provides information regarding general storm track behavior, but without the ability to separately analyze cyclones and anticyclones. This approach characterizes storm tracks as regions of high variability as estimated by, e.g., the standard deviation of the meridional wind at 200hPa; areas of high standard de-

viation indicate areas of strong storm development. This approach is similar to that in Chang and Orlanski (1993) and Berbery and Vera (1996). An Eulerian view of the vorticity at 850hPa is also examined.

The winds at 200hPa have the seasonal variability removed by subtracting the seasonal mean of each year from the seasonal data of each year. A band-pass filter of 2-6 days and a T21 truncation are applied to the Eulerian vorticity data at 850hPa.

## **2.2 Lagrangian Approach**

The Lagrangian approach examines  $\zeta_{850}$  and  $PV_{320}$  and identifies maxima that exceed  $1 \cdot 10^{-5} \text{ s}^{-1}$  and 1.0 PVU, respectively, as individual cyclones; this method can also separately identify anticyclones and track their evolutions. In this study, the propagation and evolution of each cyclone center is followed, producing tracks of individual storms.

This method computes statistics that represent storm tracks, storm strength, and other characteristics of storm tracks such as regions of strong cyclogenesis and cyclolysis. The storms examined last at least 2 days and travel farther than 1000km; these minimum criteria help to remove the possibility of capturing stationary waves alongside individual storms. The Lagrangian approach is able to identify low pressure systems earlier in their life cycles; because vorticity is less influenced by the background flow, and storm genesis regions are typically small in scale, the vorticity fields can more easily expose these regions than mean sea level pressure, the meridional wind, and other such variables.

For this approach, the vorticity and potential vorticity fields undergo filtering schemes similar to those found in Hoskins and Hodges (2002). The planetary scales with

total wavenumbers less than or equal to 5 are removed at each analysis time for  $\zeta_{850}$  and  $PV_{320}$ . A band-pass filter of 2-6.5 days is applied as well as a taper “acting as a  $\nabla^4$  smoother and having a value of 0.1 on the smallest retained scale” (Hoskins and Hodges 2002).

## Chapter 3. Results

### 3.1 Eulerian Approach

We use the Eulerian or local approach to analyze storm tracks in the Northern Hemisphere. The average position of the Northern Hemisphere high-velocity mean zonal wind (i.e., the jet stream) at 200hPa (Fig. 1) extends east from the western coast of Africa around 35°N and achieves a maximum over the western Pacific Ocean. A second maximum is centered over the eastern coast of North America around 40°N and extends northeast into the western Atlantic Ocean. The Southern Hemisphere mean zonal wind pattern (Fig. 1) exhibits a single zonally elongated maximum around 45°S in

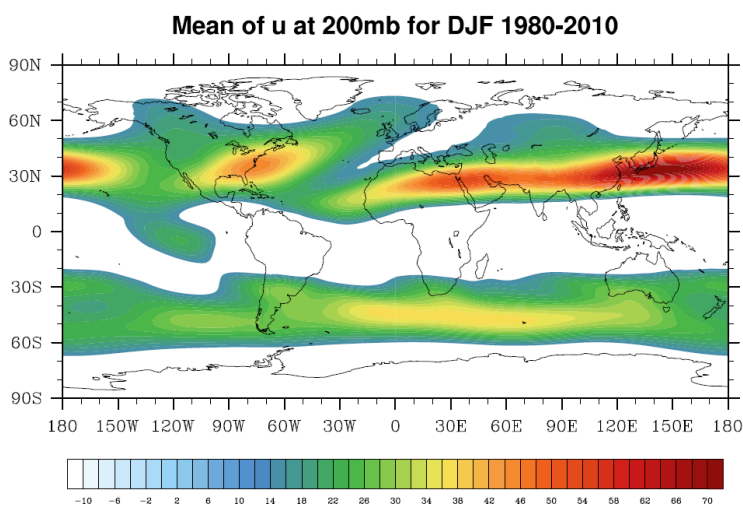


*Figure 1:* Mean zonal wind at 200hPa for DJF season from 1980-2010, global. Values less than 15.0 m/s removed for aesthetic clarity. Contour interval is 2.0 m/s.

the Southern Ocean south of the African continent. Storm tracks represented as regions of high variability of the meridional wind at 200hPa (Fig. 2A) occur on the poleward side of the jet stream in both hemispheres (Fig. 2B); for the remainder of this paper, we focus on the Northern Hemisphere.

maximum is centered over the eastern coast of North America around 40°N and extends northeast into the western Atlantic Ocean. The Southern Hemisphere mean zonal wind pattern (Fig. 1) exhibits a single zonally elongated maximum around 45°S in

Individual storm tracks are indistinguishable in the 200hPa pattern; rather, a wide latitude band of high variability extends eastward from the central North Pacific Ocean to the western coast of North America, and from the central United States to the western coast of the United Kingdom. Three centers of particularly high variability reside over the central-eastern North Pacific, the central United States, and the western North Atlantic Ocean (Fig. 2C). These areas exemplify regions of particularly strong storm development.

### Standard deviation of $v$ at 200mb for DJF 1980-2010

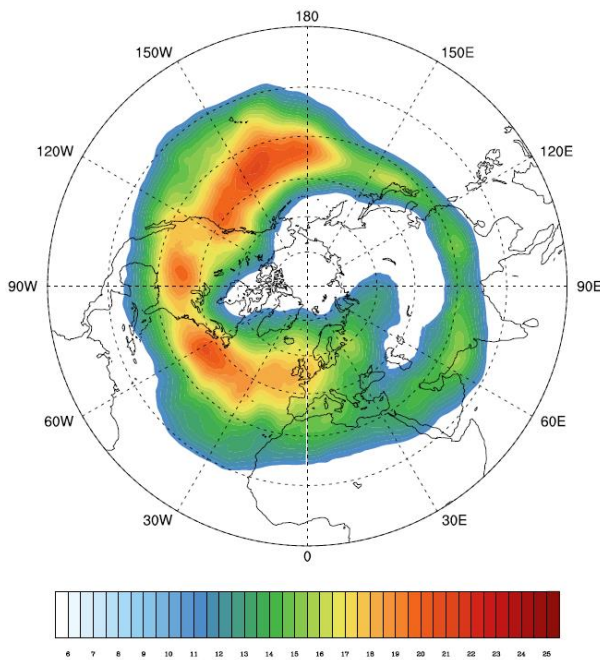


*Figure 2A:* Standard deviation of meridional wind at 200hPa for DJF season from 1980-2010 for the Northern Hemisphere. Each year's seasonal mean is removed from each year before calculation; no other filtering is applied. Values less than 11.0 m/s removed for aesthetic clarity. Contour interval is 0.5 m/s.

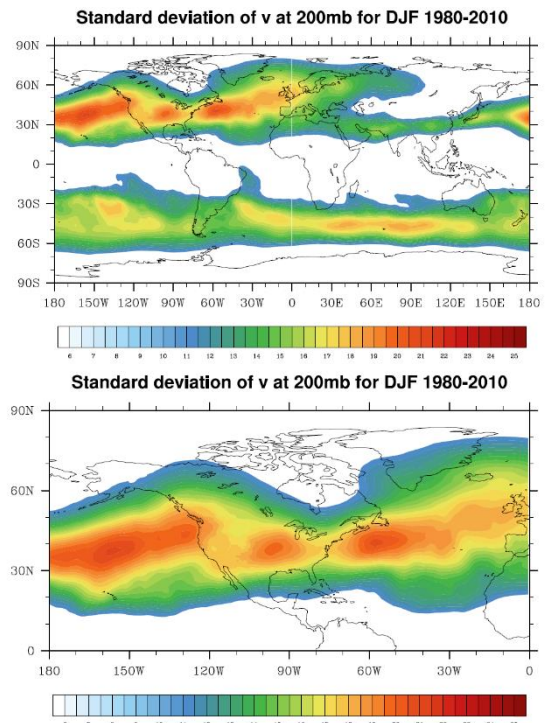


*Figure 2B (top):* A global, non-polar view of Fig. 2A. Values less than 11.0 m/s removed for aesthetic clarity. Contour interval is 0.5 m/s.

*Figure 2C (bottom):* An enlarged version of Fig. 2B concentrating over North America. Values less than 11.0 m/s removed for aesthetic clarity. Contour interval is 0.5 m/s.

We explore one such area over North America at a base point of  $38^{\circ}\text{N}$ ,  $95^{\circ}\text{W}$  located over the central United States. The base point  $38^{\circ}\text{N}$ ,  $95^{\circ}\text{W}$  was chosen because it is a maximum in the variability of the meridional wind at 200hPa. Correlation and regres-

sion techniques reveal an eastward-propagating wave characteristic of an individual storm passing over the base point (Fig. 3A). Its average longitudinal extension is 90 degrees. The wave begins with split centers over the northern Pacific Ocean in Lag -2, and

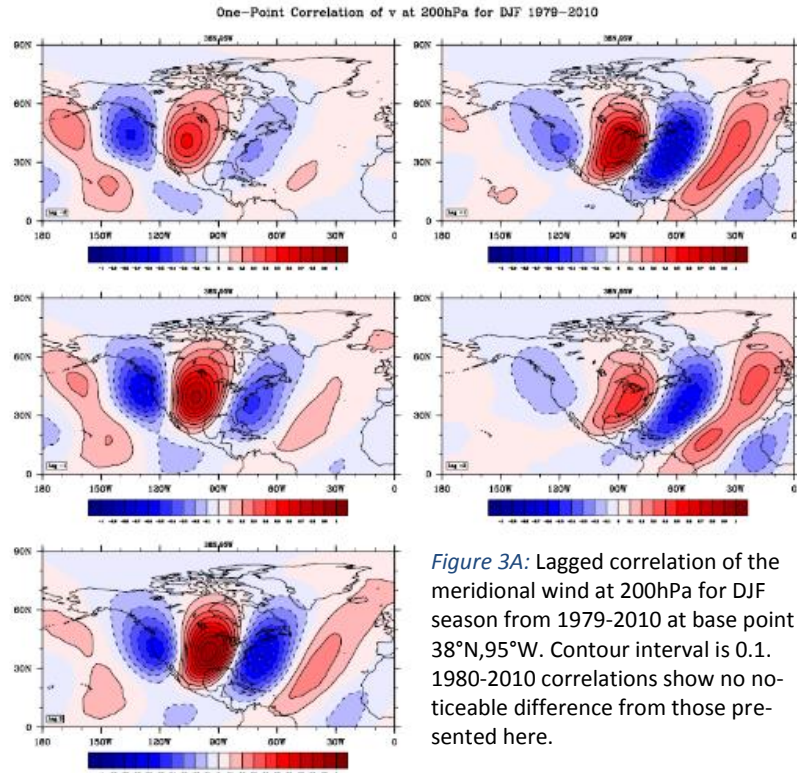


Figure 3A: Lagged correlation of the meridional wind at 200hPa for DJF season from 1979-2010 at base point  $38^{\circ}\text{N}, 95^{\circ}\text{W}$ . Contour interval is 0.1. 1980-2010 correlations show no noticeable difference from those presented here.

then develops into a high energy wave with a single center. The wave's tilt is mirrored on either side of the base point  $38^{\circ}\text{N}, 95^{\circ}\text{W}$ , exhibiting a tilt of a NNW-SSE orientation upstream and a NNE-SSW orientation downstream. The tilt of the wave increases with the wave's evolution. The energy builds as the wave propagates toward the base point, maximizing over North America at lag 0. By lag +2, the wave has propagated across North America, splitting into two centers once again when it reaches the western coasts of Europe and Africa. In these areas the 200hPa storm track diverges into two separate tracks: one extends northeast into Europe and northern Russia, and the other extends across the Middle East along  $30^{\circ}\text{N}$ . As the wave moves over the Atlantic Ocean, its energy begins to dissipate, further weakening as the wave splits.

Through similar local diagnostics, we find that this wave pattern leaves a signature in surface precipitation (Fig. 3B). A wave propagates eastward and crosses the North

American continent. This wave shares similar characteristics with that produced from the 200hPa meridional wind; however, the precipitation wave does not show split wave centers at any lag, nor does the tilt of this wave shift from its NNE-SSW orientation. As this wave

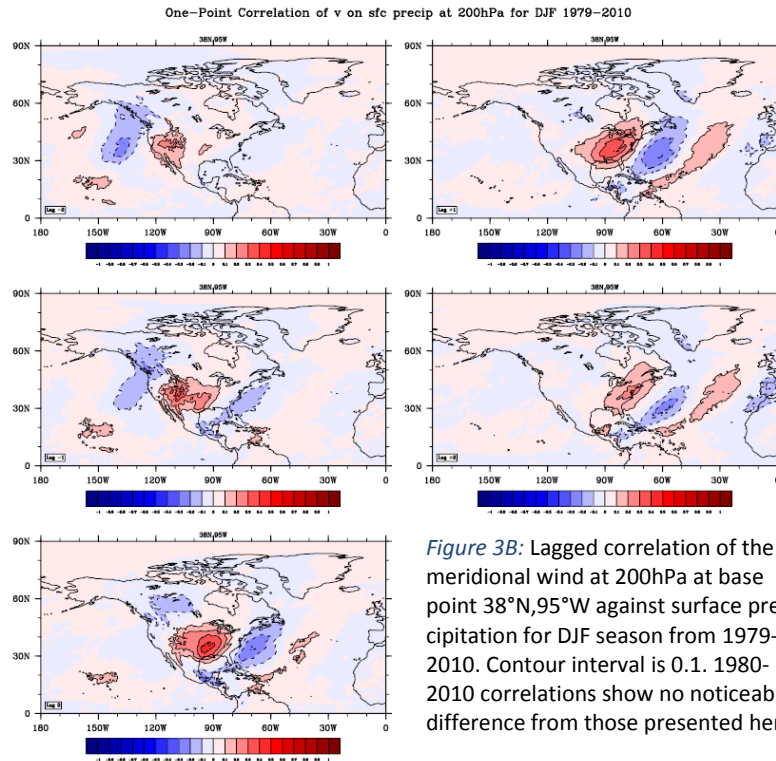
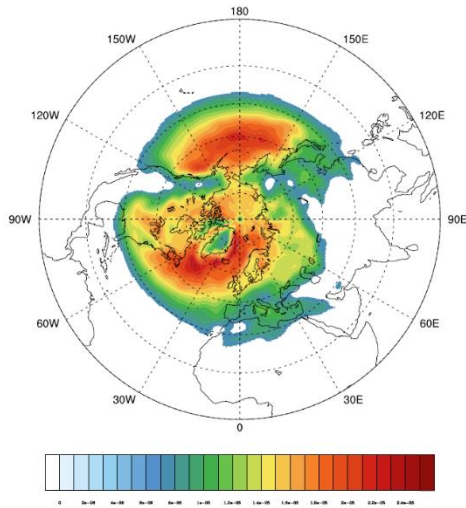


Figure 3B: Lagged correlation of the meridional wind at 200hPa at base point 38°N,95°W against surface precipitation for DJF season from 1979-2010. Contour interval is 0.1. 1980-2010 correlations show no noticeable difference from those presented here.

evolves, it elongates meridionally, and its tilt increases to a NE-SW direction. From lags -2 to 0, the wave energy rises. Once it crosses into the Atlantic Ocean, the energy rapidly dissolves. In lag +2, this wave follows a path that lies between the split centers of the 200hPa wave train; by the time this wave reaches the western shores of Europe and northern Africa, little to no signal of the upper tropospheric meridional wind pattern remains in the precipitation pattern.

Storm tracks represented by the variability of vorticity at 850hPa are also examined (Fig. 4). Two individual regions of vorticity variability are discerned: one extends west to east across the North Pacific Ocean from Japan to the west coast of Canada, and the other extends southwest to northeast across the North Atlantic Ocean from eastern North America to the Norwegian Sea. Regressions are computed to ascertain the structure of an individual wave passing over the base point 38°N, 95°W (Fig. 5A). The wave

**Standard deviation of vor at 850mb for DJF 1980-2010**



*Figure 4:* Standard deviation of vorticity at 850hPa for DJF season from 1980-2010 for the Northern Hemisphere. Band-pass filter is applied from 2-6 days. T21 truncation is also applied (i.e., all wavenumbers greater than or equal to 21 are removed). Values less than  $7.0 \cdot 10^{-6}$  1/s removed for aesthetic clarity. Contour interval is  $0.1 \cdot 10^{-5}$  1/s.

produced loses energy when it shifts from a NE-SW tilt to a NNE-SSW tilt as it propagates eastward from the base point to the Atlantic Ocean. Compared to the synoptic nature of the wave train at 200hPa, the low-level vorticity wave reveals smaller scales; this wave is confined to the latitudes bounding the United States, contrary to the 200hPa wave train that spreads meridionally from Mexico to northern Canada. Smaller scaled features are also shown in the single-

point regression of vorticity onto surface precipitation (Fig. 5B). Regional precipitation signals are revealed as the wave produced propagates eastward from the base point and disappears over the eastern North Atlantic Ocean. Enhanced precipitation from orographic effects on the western coast of North America is also observed. The tilt of the wave shifts from N-S to NNE-SSW; the wave maintains its energy until it crosses into the eastern half of the North Atlantic Ocean where it rapidly dissipates.

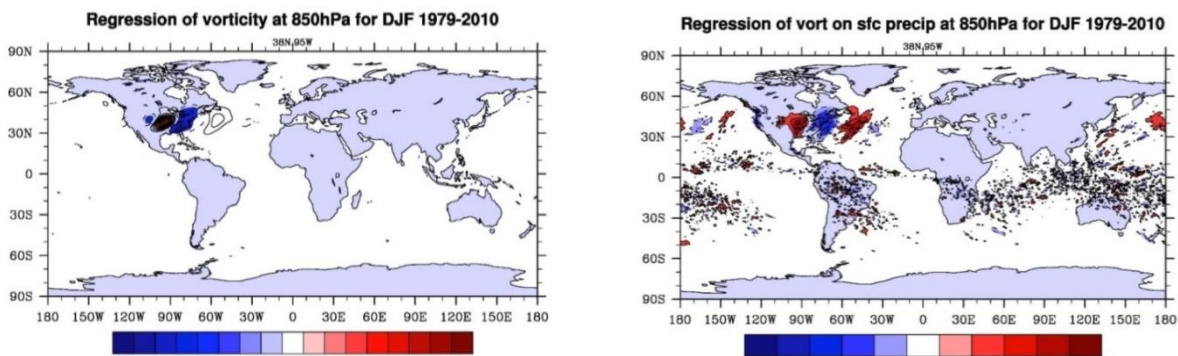


*Figure 5:* Regression of A) Eulerian filtered vorticity at 850hPa (left), and B) Eulerian filtered vorticity at 850hPa onto surface precipitation rate field (right), at base point 38°N,95°W for DJF season from 1979-2010. Values -0.2 to 0.2 are removed for aesthetic clarity. Contour interval is 0.1 and 0.2 for Figs. 5A and 5B, respectively. 1980-2010 regressions show no noticeable difference from those presented here.

### 3.2 Lagrangian Approach

The analysis centers on two variables: vorticity at 850hPa and potential vorticity at  $\theta=320\text{K}$ . A variety of statistics is computed as in Hoskins and Hodges (2002) to diagnose and characterize storm tracks and their behaviors in the Northern Hemisphere, focusing on the boreal winter season.

Individual tracks of storms are estimated as single points derived from spherical kernel estimators with local kernel functions, resulting in a set of data that can be normalized to a PDF. A brief description of each diagnostic is presented here, followed in the next sections by a deeper analysis of each storm track.

The statistic labeled track density as defined by Hoskins and Hodges (2002) is the density of these single track points and is the storm track pattern. Figures 6A and 6B show the tracks of individual storms identified in 1980 from the variables  $\zeta_{850}$  and  $PV_{320}$ , respectively. Figure 6C shows the tracks of individual storms identified from the  $PV_{320}$  field from 1980-2010.

The track density statistic represents the storm track pattern in the Northern Hemisphere. The pattern of  $\zeta_{850}$  (Fig. 7A) reveals four separate and distinct tracks mostly residing above  $30^\circ\text{N}$ . The pattern of  $PV_{320}$  (Fig. 7B) shows three distinct tracks confined between latitudes  $30^\circ\text{N}$  and  $60^\circ\text{N}$ .

**1980 DJF vorticity trajectories**

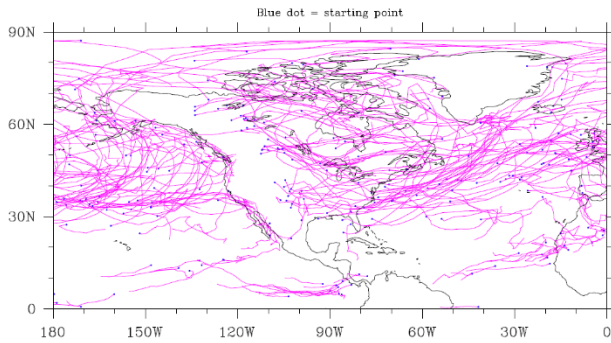


*Figure 6A:* Individual storm tracks from vorticity at 850hPa that last longer than 2 days and travel further than 1000 km over North America in the DJF season for **1980**. Blue dots mark the starting points of each track. These storms are identified and tracked using the Lagrangian approach via TRACK.

**1980 DJF pv trajectories**

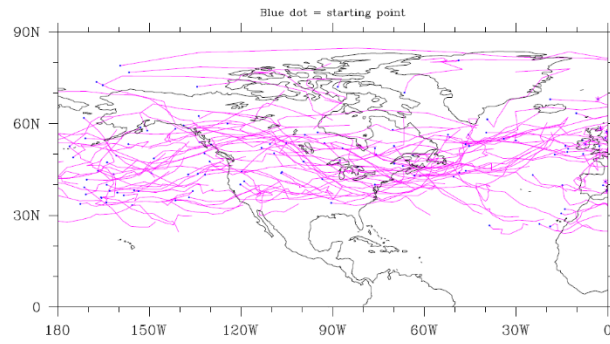


*Figure 6B:* Individual storm tracks from potential vorticity at  $\theta=320K$  that last longer than 2 days and travel further than 1000 km over North America in the DJF season for **1980**. Blue dots mark the starting points of each track. These storms are identified and tracked using the Lagrangian approach via TRACK.

**1980-2010 DJF pv trajectories**

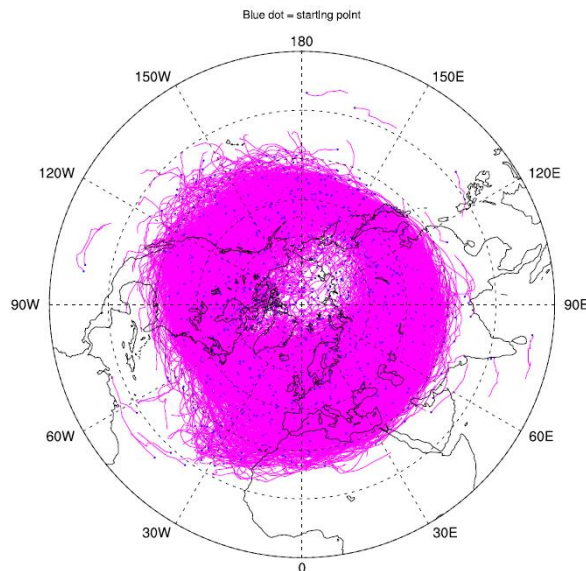


*Figure 6C:* A Northern Hemisphere view of *Fig. 6B* but from **1980-2010**.

The mean intensity statistic denotes the average strength of the storms that comprise each storm track. The  $\zeta_{850}$  mean intensity statistic (Fig. 8A) shows two regions of strong storms concentrated over the northern Pacific and Atlantic Ocean basins. The  $PV_{320}$  mean intensity pattern (Fig. 8B) reveals a band of storm track strength reaching eastward from the central North Pacific Ocean to just west of the Mediterranean Sea.

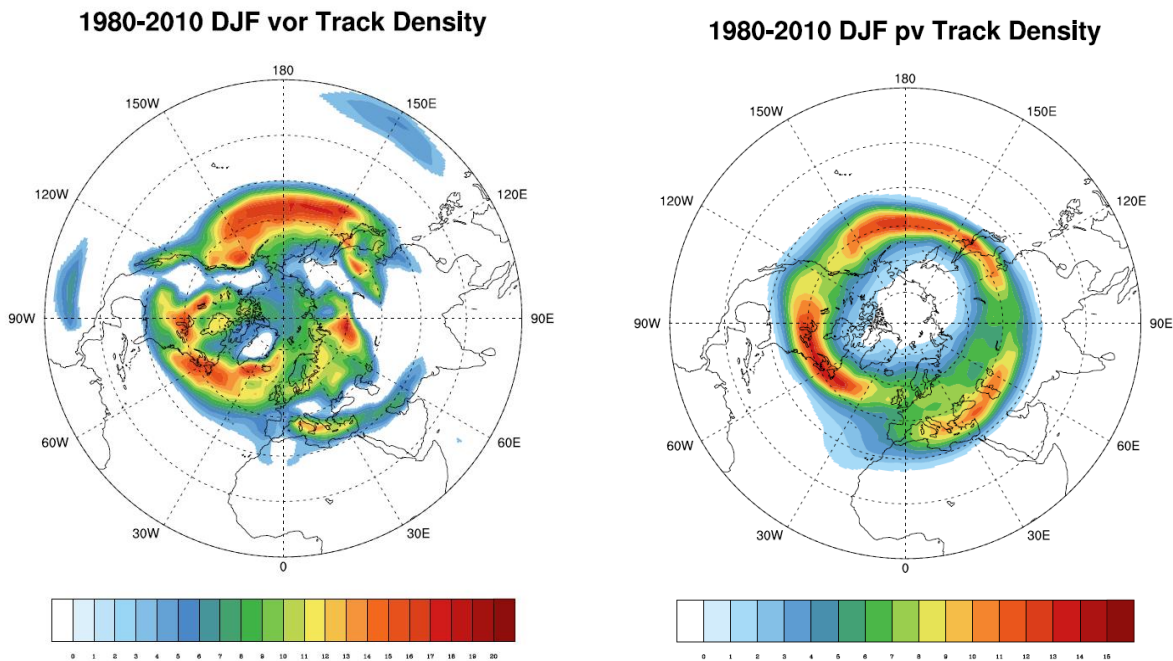


Figure 7: Lagrangian track density of A) vorticity at 850hPa (left), and B) potential vorticity at  $\theta=320\text{K}$  (right), for the DJF season from 1980-2010. Individual storm tracks are represented by single estimation points using kernel estimators. This shows the density of individual tracks, as represented by these points, thus displaying the storm track pattern for the DJF season in the Northern Hemisphere. Values less than 3.0 and 1.0 are removed for aesthetic clarity from Figs. 7A and 7B, respectively. Contour interval is 1.0 number of storms per month with a unit area of  $10^6 \text{ km}^2$  [ $5^\circ$  spherical cap] for both figures.

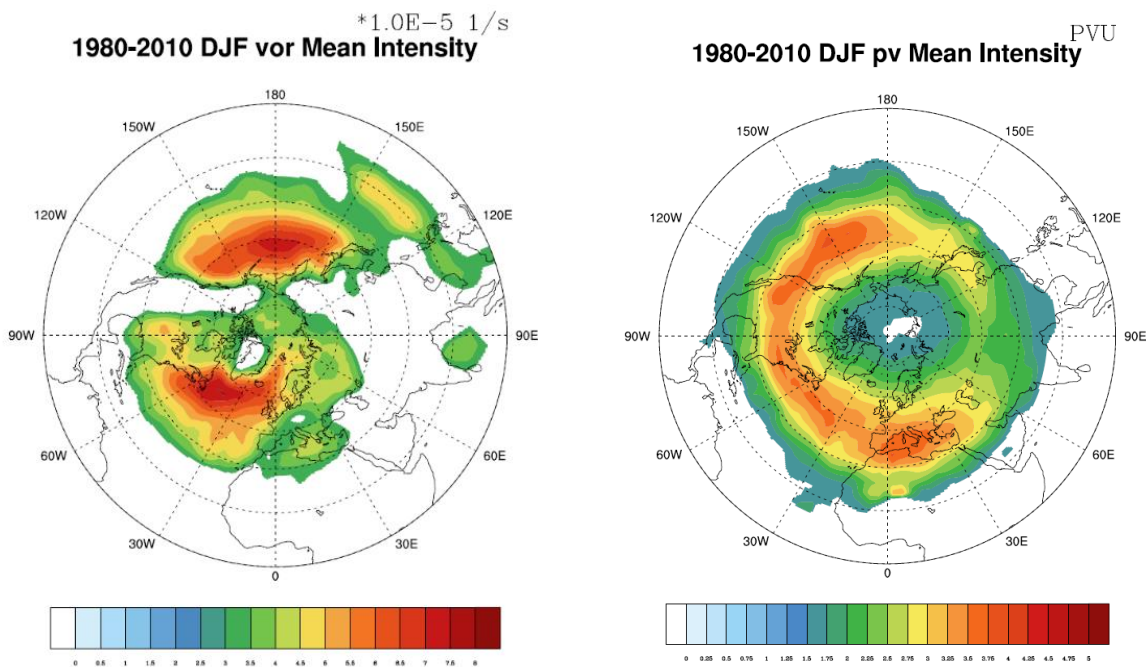


Figure 8A (left): Lagrangian mean intensity of the Northern Hemisphere storm track patterns of vorticity at 850hPa as seen in Fig. 7A for the DJF season from 1980-2010. This shows the average strength of the storm tracks. Values less than  $3.0 \times 10^{-5} \text{ 1/s}$  are removed for aesthetic clarity. Contour interval is  $0.5 \times 10^{-5} \text{ 1/s}$ .

Figure 8B (right): Lagrangian mean intensity of the Northern Hemisphere storm track patterns of potential vorticity at  $\theta=320\text{K}$  as seen in Fig. 7B for the DJF season from 1980-2010. This shows the average strength of the storm tracks. Values less than 1.5 PVU are removed for aesthetic clarity. Contour interval is 0.25 PVU.

The genesis density statistic is computed using the points of origin of each cyclone identified; in other words, it highlights regions of cyclogenesis. The  $\zeta_{850}$  cyclogenesis pattern (Fig. 9A) exhibits isolated regions of cyclogenesis. The  $PV_{320}$  cyclogenesis pattern (Fig. 9B) reveals cyclogenesis regions that are more zonally oriented and appear to follow the  $PV_{320}$  storm track pattern.

The lysis density statistic is computed using the points at which each cyclone disappears; in other words, it highlights regions of cyclolysis. The  $\zeta_{850}$  lysis density statistic (Fig. 10A) shows concentrated regions of cyclolysis, while the  $PV_{320}$  lysis density pattern (Fig. 10B) reveals more zonally oriented regions of cyclolysis that seem to follow the  $PV_{320}$  storm track pattern.

This approach allows for the identification of precipitation associated with an individual storm center. Precipitation that falls within a specified spherical radius of an individual storm center is considered to be associated with that particular storm; the spherical radius used in this study is  $5^\circ$ ; this precipitation is referred to as storm-associated precipitation. We compute the mean intensity of the precipitation associated with storms derived from the  $\zeta_{850}$  and  $PV_{320}$  fields (Figs. 11A and 11B, respectively).

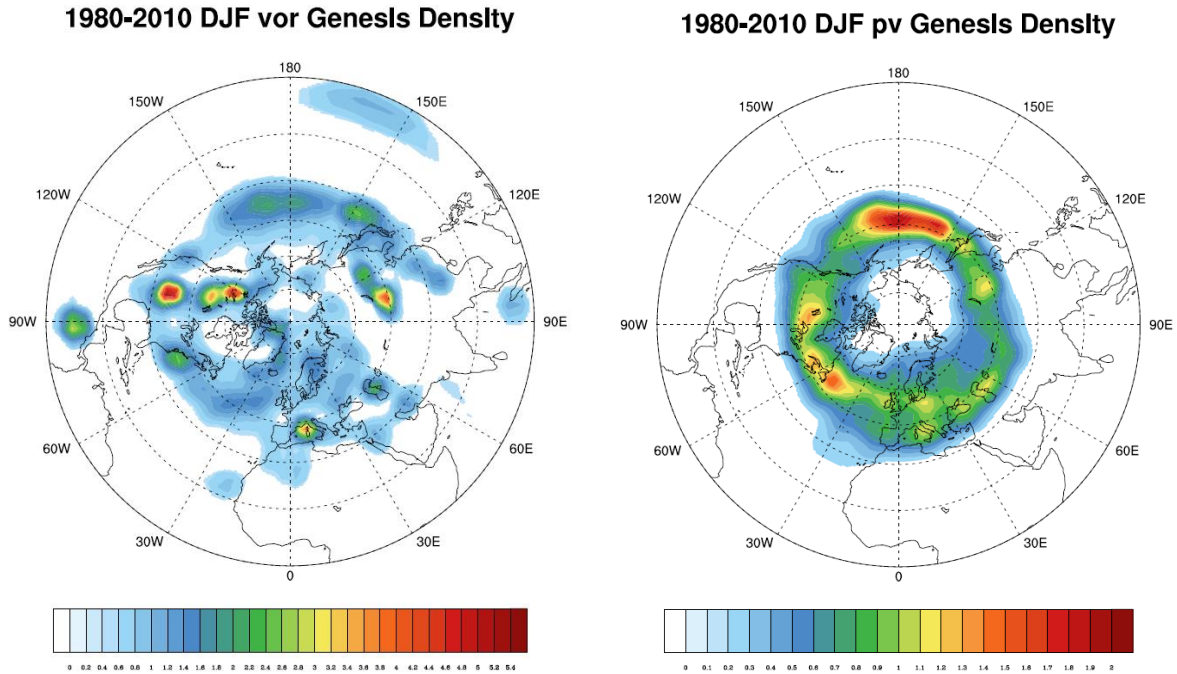


Figure 9: Lagrangian genesis density for A) vorticity at 850hPa (left), and B) potential vorticity at  $\theta=320\text{K}$  (right), for the Northern Hemisphere storm track patterns (as seen in Figs. 7A and 7B, respectively) for the DJF season from 1980-2010. This highlights regions of cyclogenesis using the starting points of each track to compute the density. Values less than 0.5 and 0.2 are removed from Figs. 10A and 10B, respectively, for aesthetic clarity. Contour interval is 0.2 and 0.1 number of storms per month with a unit area of  $10^6 \text{ km}^2$  [ $5^\circ$  spherical cap] for Figs. 10A and 10B, respectively.

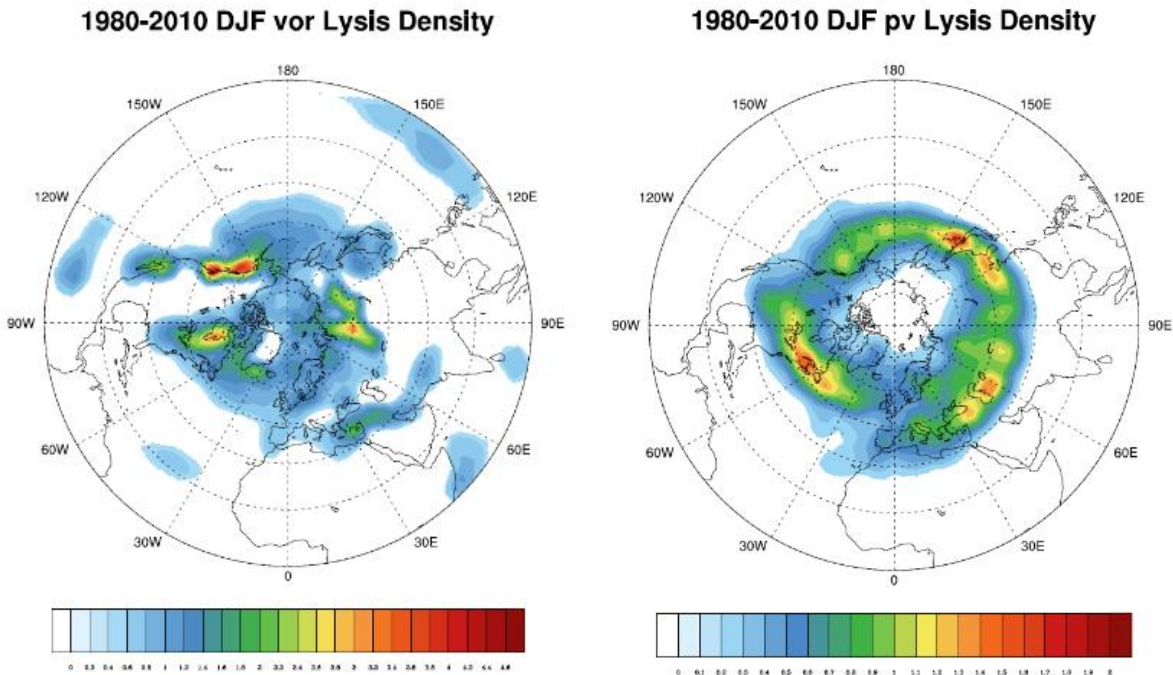
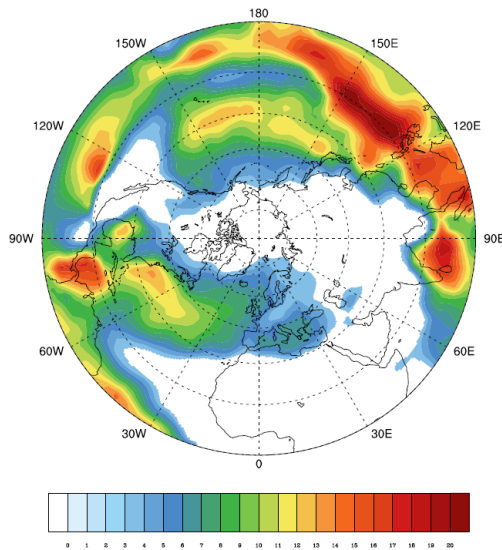
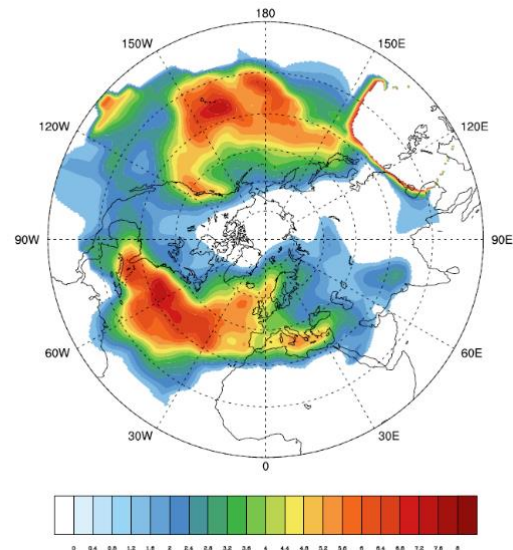


Figure 10: Lagrangian lysis density for A) vorticity at 850hPa (left), and B) potential vorticity at  $\theta=320\text{K}$  (right), for the Northern Hemisphere storm track patterns (as seen in Figs. 7A and 7B, respectively) for the DJF season from 1980-2010. This highlights regions of cyclolysis using the end points of each track to compute the density. Values less than 0.5 and 0.2 are removed from Figs. 10A and 10B, respectively, for aesthetic clarity. Contour interval is 0.2 and 0.1 number of storms per month with a unit area of  $10^6 \text{ km}^2$  [ $5^\circ$  spherical cap] for Figs. 10A and 10B, respectively.

1980-2010 DJF Mean Intensity of PR associated with vor 1980-2010 DJF Mean Intensity of PR associated with PV



*Figure 11A:* Lagrangian mean intensity of the Northern Hemisphere precipitation associated with the vorticity at 850hPa storm track pattern (as seen in **Fig. 7A**) for the DJF season from 1980-2010. This shows the average precipitation rate associated with storms that travel farther than 1000km and last longer than 2 days. Values less than 3.0 mm/day are removed for aesthetic clarity. Contour interval is 1.0 mm/day.



*Figure 11B:* Lagrangian mean intensity of the Northern Hemisphere precipitation associated with the potential vorticity at  $\theta=320K$  storm track pattern (as seen in **Fig. 7B**) for the DJF season from 1980-2010. This shows the average precipitation rate associated with storms that travel farther than 1000km and last longer than 2 days. Values less than 1.2 mm/day and greater than 8.0 mm/day are removed for clarity. Contour interval is 0.02 mm/day.

### 3.2.1 Pacific Storm Track

The  $\zeta_{850}$  Pacific storm track shown in Fig. 7A resides primarily over the North Pacific Ocean, extending from eastern Asia to the western coast of North America. The greatest number of storms in the Northern Hemisphere DJF season occurs within the western half of the Pacific track.

From the mean intensity pattern (Fig. 8A) we see that its peak strength occurs over the western half of the Pacific Ocean. Two cyclogenesis regions of similar magnitude are shown to reside east of Japan and in the central North Pacific Ocean (Fig. 9A).

This track reveals small scaled features such as the low latitude extension of the eastern end of the Pacific track into southern California, USA. Fig. 10A shows that the

two regions where cyclolysis occurs the most are located over the western coast of Canada, implying that many storms originating from the Pacific track dissipate there. Several storms from the Pacific track also decay in the Southern California, USA area, coinciding with the low latitude extension of that storm track.

The  $PV_{320}$  view of the Pacific storm track is shown in Fig. 7B, and spreads across the North Pacific Ocean from eastern Asia to the east of North America. The greatest number of storms within the Pacific track occurs over the western-central North Pacific Ocean. Fig. 8B reveals the largest peak of mean intensity in the Northern Hemisphere to be related to the Pacific track, and it reaches a maximum intensity in the eastern half of the North Pacific Ocean. The most dense region of cyclogenesis (Fig. 9B) is that over the North Pacific Ocean; this region spreads eastward from east of Japan to the eastern North Pacific Ocean and is associated with the Pacific track. The highest peaks in density that are associated with the Pacific track reside west of and over northern Japan. In Fig. 10B we see that a band of relatively lower lysis density reaches eastward across the North Pacific Ocean, peaking in the central North Pacific and off the coast of western North America. The  $PV_{320}$  cyclolysis pattern does not show the unusually high lysis density peaks on the western coast of Canada shown in the  $\zeta_{850}$  pattern.

As expected, the  $\zeta_{850}$  storm-associated precipitation pattern (Fig. 11A) reveals the highest rate of precipitation over the warm pool in the western tropical Pacific Ocean. Also as expected, bands of high precipitation circle the globe in the lower latitudes (i.e., the tropics), following the Intertropical Convergence Zone (ITCZ). In the mid-latitudes, precipitation patterns over the Pacific Ocean span between  $15^{\circ}\text{N}$  and  $45^{\circ}\text{N}$ , approximate-

ly 10-15° south of the  $\zeta_{850}$  Pacific storm track. The local peaks in precipitation associated with the Pacific track occur east of Japan and north of Hawaii, USA.

Fig. 11B reveals that the highest rate of precipitation associated with storms identified from  $PV_{320}$  occurs over the warm pool region in the western tropical Pacific Ocean. The values in this region are masked out because the extremely large magnitude of precipitation in this region is an artifact of the computation, since the 320K surface intersects the Earth's surface and would be below it. Aside from differences in the tropics, the  $PV_{320}$  storm-associated precipitation pattern follows a somewhat similar pattern to that of  $\zeta_{850}$ . One region of  $PV_{320}$  storm-associated precipitation that is dominant in the Northern Hemisphere occurs over the Pacific Ocean, and is associated with the Pacific storm track. This pattern lies between 15°N and 45°N except for its eastern end, which extends into the high latitudes beyond 45°N. It peaks in precipitation in two locations: one occurs just northwest of Hawaii, USA and the other occurs west of Hawaii, USA around the dateline.

The  $PV_{320}$  storm-associated precipitation pattern highlights the higher latitude extensions of precipitation, underlining the effect that storms from the Pacific storm track have on precipitation above the mid-latitudes in the Northern Hemisphere. This is exemplified in the eastern end of the precipitation pattern related to the Pacific track (Fig. 11B), where the existence of the local peak in precipitation is likely due to orographic effects associated with the Rocky Mountains.

### **3.2.1 North American-Atlantic (NAA) Storm Track**

The  $\zeta_{850}$  NAA storm track seen in Fig. 7A extends northeast from the central North American continent across the North Atlantic Ocean and into the Greenland Sea.

This track reveals small scale features such as the high latitude extension of the eastern end of the Atlantic track into the Greenland Sea. The highest number of storms in the NAA track occurs over the eastern coast of North America and southwest of Iceland. From the mean intensity pattern in Fig. 8A we see that one of the strongest storm tracks is the NAA track; its maximum strength is similar in magnitude to that of the Pacific track and occurs over the western half of the North Atlantic Ocean. Right away we notice three isolated regions of high genesis density in the  $\zeta_{850}$  cyclogenesis pattern on the leeward side of the Rocky Mountains in North America (Fig. 9A). The unusually high densities here could perhaps incorporate stationary waves; further study is needed to verify this. There is a region of relatively high genesis density off the eastern coast of North America that is thought to exist because of the Nor'easter storms that develop there in the boreal winter; again, more analysis is required for verification. The  $\zeta_{850}$  cyclolysis pattern (Fig. 10A) reveals a few isolated regions of high lysis density over North America and Eurasia. Many storms from the NAA storm track dissipate east of the Hudson Bay in Canada and also south of Greenland.

The  $PV_{320}$  NAA storm track seen in Fig. 7B extends from the western-central North American continent to the western North Atlantic basin. The NAA track appears to have the greatest number of its storms occur around the Great Lakes region and also over the northeastern coast of North America. The peak mean intensity of the NAA track (Fig. 8B) occurs over the western North Atlantic Ocean. Fig. 9B shows that the most dense cyclogenesis regions associated with the NAA storm track spread from central North America to the western North Atlantic Ocean. Fig. 10B shows that the cyclolysis pattern

associated with the NAA track spreads across the northeastern North American continent into the North Atlantic Ocean.

In the mid-latitudes, Fig. 11A reveals that the  $\zeta_{850}$  storm-associated precipitation pattern over the Atlantic Ocean spans between 15°N and 45°N, approximately 10-15° south of its respective storm track. The local peaks in precipitation associated with the NAA storm track occur in the Gulf of Mexico and east of the United States.

A dominant region of  $PV_{320}$  storm-associated precipitation in the Northern Hemisphere (Fig. 11B) occurs over the Atlantic Ocean. This precipitation pattern lies between 15°N and 45°N except for the eastern end of the pattern, which extends into the high latitudes beyond 45°N. The  $PV_{320}$  precipitation pattern associated with the NAA storm track peaks southeast of Florida, USA and east of North America. As the pattern approaches Europe, it extends northeastward toward Iceland and the Norwegian Sea, with a local peak residing west of the United Kingdom.

### **3.2.2 Mediterranean Storm Track and Other Features**

The  $\zeta_{850}$  Mediterranean storm track shown in Fig. 7A extends east across the entire Mediterranean Sea into the Middle East. The majority of storms that originate in the Mediterranean track travel over the eastern half of the Mediterranean Sea. Fig. 8A reveals the mean intensity of the Mediterranean track to be weak even when compared to the weak signal captured over the warm pool region in the western tropical Pacific Ocean. A region of high genesis density exists over western Italy in the Mediterranean Sea, and another exists south of Lake Baikal in Russia (Fig. 9A). Fig. 10A reveals that storms fol-

lowing the Mediterranean track disappear southeast from the eastern edge of the Mediterranean Sea to the Persian Gulf.

The  $PV_{320}$  Mediterranean storm track seen in Fig. 7B reaches eastward across the entire Mediterranean Sea to east of the Caspian Sea. The majority of storms that originate in the Mediterranean track travel over the eastern half of the Mediterranean Sea. The peak mean intensity of the Mediterranean track (Fig. 8B) is similar in magnitude to that of the  $PV_{320}$  NAA track and occurs over the western half of the Mediterranean Sea. Fig. 9B shows that the Mediterranean track has the fewest number of cyclogenesis events when compared to the  $PV_{320}$  Pacific and NAA tracks and spreads eastward from the Mediterranean Sea to the Middle East. The region south of Lake Baikal in Russia is vividly captured in the  $\zeta_{850}$  genesis pattern in Fig. 9A but is not as pronounced in the  $PV_{320}$  pattern. The peaks in lysis density related to the Mediterranean track occur southeast of the Black Sea and east of the Caspian Sea, and are more isolated than those related to the  $PV_{320}$  Pacific and NAA tracks (Fig. 10B).

There is a slight hint of the  $\zeta_{850}$  Mediterranean storm track in its corresponding precipitation pattern over the Mediterranean Sea, although its magnitude is about half of the local maxima in precipitation in both the  $\zeta_{850}$  Pacific and NAA patterns (Fig. 11A).

The precipitation rate associated with the  $PV_{320}$  Mediterranean track is low compared to those related to the  $PV_{320}$  Pacific and NAA tracks (Fig. 11B). The Mediterranean precipitation reaches a maximum in the middle of the Mediterranean Sea; this region spreads from west of Spain to south of the Black Sea.

The  $\zeta_{850}$  storm track pattern in Fig. 7A reveals a fourth storm track in Siberia, which extends southwestward from Siberia until approximately  $45^\circ\text{N}$ . The magnitude of this track is comparable to the  $\zeta_{850}$  NAA storm track. The  $\zeta_{850}$  cyclolysis pattern (Fig. 10A) shows that many storms traveling across Siberia tend to disappear there. However, note that the  $\text{PV}_{320}$  storm track pattern (Fig. 7B) does not display any hint of a Siberian storm track. There is speculation that the high magnitude of densities in Siberia highlighted in the  $\zeta_{850}$  storm track and  $\zeta_{850}$  cyclolysis pattern exist due to orographic effects or may be a mathematical product; these theories are supported by the lack of any notable cyclogenesis regions in or near Siberia in the cyclogenesis patterns of  $\zeta_{850}$  and  $\text{PV}_{320}$  (Figs. 9A and 9B, respectively). It is suggested that the possible existence of a Siberian track be further studied to verify these theories.

## Chapter 4. Discussion

### 4.1 Comparisons between variables using Eulerian Approach

The storm track at 200hPa is displayed in the Northern Hemisphere as one large track that spans the entire globe. This track is slightly poleward of the 200hPa jet stream and has a spatial pattern that is similar to the jet stream but offset to the east by about 30° degrees longitude. Small spatial scales are not captured in part because of the vertical distance between the 200hPa pressure level and the earth's surface. The use of variables at this upper tropospheric level via the Eulerian approach is not recommended for detecting storms at stages of development that occur on small scales.

The storm track pattern derived from the vorticity at 850hPa reveals two tracks that are clearly positioned poleward of the jet stream at 200hPa. Some small scaled features are captured as, e.g., peaks of strong storm tracks that occur in the central and eastern North Pacific basin.

### 4.2 Comparisons between Eulerian and Lagrangian Approaches

The  $\zeta_{850}$  storm track pattern from the Lagrangian approach somewhat spatially resembles the Eulerian storm track at 200hPa. The  $\zeta_{850}$  mean intensity more closely resembles the standard deviation of the Eulerian vorticity field at 850hPa than it does the  $\zeta_{850}$  track density pattern. This is reasonable because the  $\zeta_{850}$  mean intensity is derived from the raw vorticity field at 850hPa, which is filtered in a similar fashion to that of the Eulerian low-level vorticity field. At first it seems that the Eulerian vorticity pattern exhibits more small scaled features than the Lagrangian  $\zeta_{850}$  mean intensity pattern; however, the Eulerian field appears to be biased toward higher latitudes as it entirely misses the storm strength over the warm pool region captured by the Lagrangian  $\zeta_{850}$  mean intensity pat-

tern. The Lagrangian  $\zeta_{850}$  field and the Eulerian vorticity best match in the mid-latitudes. Therefore, it is suggested that the standard deviation of the filtered vorticity field at 850hPa is better suited for the analysis of storm intensity rather than storm tracks themselves in the mid-latitudes in the Northern Hemisphere. The Siberian track highlighted in the  $\zeta_{850}$  track density pattern does not appear in the Eulerian 200hPa pattern.

The  $PV_{320}$  track density pattern shares only one notable commonality with the storm track pattern at 200hPa: they both flow along and on either side of  $45^\circ\text{N}$ . The  $PV_{320}$  mean intensity pattern only slightly resembles the storm track pattern at 200hPa. The spatial structure of the  $PV_{320}$  pattern extends from  $30^\circ\text{N}$  to  $60^\circ\text{N}$  from the western North Pacific Ocean to east of the Mediterranean Sea; the 200hPa storm track pattern shares the same latitudinal extension in the eastern North Pacific and North Atlantic basins, narrowing slightly over North America. The  $PV_{320}$  mean intensity pattern reaches a maximum in the western North Pacific Ocean just a few degrees east of the local maximum in variability at 200hPa. The local maxima in  $PV_{320}$  mean intensity over the North Atlantic basin reside near the single maximum in variability over the same basin at 200hPa. Other than these spatial similarities, the two patterns are dissimilar.

#### **4.2.1 Pacific Storm Track**

The maxima in track density in the  $\zeta_{850}$  Pacific storm track are 5-10 degrees poleward of the strong Eulerian storm tracks in the Pacific; this is reflected over the North Pacific Ocean. The western end of the Pacific storm track shown in the  $\zeta_{850}$  track density pattern displays two extensions into the Asian continent, one emerging from eastern Asia and the other from south of Japan. These extensions are represented as one thin zonal area of average intensity in the 200hPa pattern. The 200hPa pattern does not capture the

maximum in  $\zeta_{850}$  track density in the western Pacific track; instead, the 200hPa pattern shows an increase in the track's strength in this region only after it crosses the dateline in the North Pacific Ocean, contrasting the track density field.

The  $\zeta_{850}$  track density pattern resembles the storm track pattern derived from the Eulerian filtered vorticity field at 850hPa. The Pacific storm track is more clearly defined in the Eulerian vorticity pattern, though it resides poleward of the Pacific track shown in the  $\zeta_{850}$  track density. The low latitude extensions of the eastern part of the Pacific track in the  $\zeta_{850}$  storm track pattern are not well-represented in the Eulerian vorticity pattern. It appears that this Eulerian vorticity field is biased toward mid- and high-latitudes, underestimating the storm track strength in lower latitudes and overestimating the strength in high latitudes, especially above 60°N.

The  $PV_{320}$  pattern is confined to a much narrower band of latitudes, and each storm track in this pattern is separate and well-defined as compared to the pattern at 200hPa. The Pacific track in the  $PV_{320}$  pattern exhibits a maximum in storm track density over Japan and another just east of the dateline, whereas the high variability in the 200hPa pattern is concentrated in the eastern half of the North Pacific basin with two local maxima occurring north of Hawaii and just offshore of the western coast of Canada.

#### **4.2.2 North American-Atlantic Storm Track**

The peaks of high track density in the  $\zeta_{850}$  NAA storm track are 5-10 degrees poleward of the strong Eulerian storm tracks over North America and the Atlantic Ocean; this is exemplified over the North American continent and in the west North Atlantic

Ocean. Over the North Atlantic Ocean, the pattern of 200hPa variability is more zonally oriented than the  $\zeta_{850}$  NAA storm track.

The NAA track is generally outlined in the Eulerian vorticity pattern. Its strength over the North Atlantic Ocean resembles that shown in the  $\zeta_{850}$  track density; however, the strength shown over the North American continent is underestimated in the low-level vorticity pattern. This pattern also overestimates the strength of the NAA track east of Greenland, where it proceeds to extend east to Siberia.

The NAA track in the  $PV_{320}$  pattern reveals a track density maximum near the Great Lakes and another along the eastern coast of North America. A maximum in 200hPa variability occurs over the central United States, and another occurs offshore of the eastern North American coast.

### 4.2.3 Mediterranean Storm Track

The Mediterranean track highlighted in the  $\zeta_{850}$  track density pattern does not appear in the 200hPa pattern; instead, a thin extension of 200hPa variability in the Middle East/Indian regions increases slightly in strength, contrasting the  $\zeta_{850}$  track density field where there exists no such increase. The Mediterranean storm track in the Lagrangian  $\zeta_{850}$  pattern is not well-represented in the Eulerian vorticity pattern. It appears that this Eulerian vorticity field is biased toward mid- and high-latitudes, underestimating the storm track strength in lower latitudes and overestimating the strength in high latitudes.

The 200hPa pattern does not exhibit any region of particularly high variability near the Mediterranean Sea; this contrasts the noticeable Mediterranean track shown in the  $PV_{320}$  track density pattern.

### 4.3 Lagrangian comparisons between $\zeta_{850}$ and $PV_{320}$

We compare the storm track patterns of  $\zeta_{850}$  and  $PV_{320}$  to their respective patterns of storm-associated precipitation. We also compare the mean intensity patterns of  $\zeta_{850}$  and  $PV_{320}$  to their respective patterns of storm-associated precipitation.

The region of high track density over Siberia highlighted in the  $\zeta_{850}$  storm track pattern has very little precipitation associated with it, further suggesting that this storm track does not physically exist.

The relations between storm tracks and precipitation described below do not appear to occur in the tropics, though further analysis is suggested for verification.

#### 4.3.1 Pacific Storm Track

The precipitation pattern associated with the Pacific storm track of  $\zeta_{850}$  resides equatorward of that storm track. The poleward gradient of this precipitation pattern lies within the Pacific track. The precipitation peaks north of Hawaii, USA and resides equatorward of the Pacific track. The peak east of Japan resides within the western part of the Pacific track.

The precipitation pattern associated with the Pacific storm track of  $PV_{320}$  resides equatorward of that storm track. The poleward gradient of this precipitation pattern lies within the  $PV_{320}$  Pacific track. Two precipitation peaks occur east of Japan and north of Hawaii, USA and reside equatorward of the Pacific storm track. The precipitation peak just west of North America lies between the eastern end of the Pacific track and the western end of the  $PV_{320}$  NAA track. This enhanced precipitation signal can in part be explained by orographic effects; because of the high orography of the Rocky Mountains,

Pacific storms propagating eastward are forced to slow and precipitate over the west coast of North America for a longer period of time than their usual propagation speeds would normally allow. Unexpectedly, this pattern is not noticeably captured in the  $\zeta_{850}$  storm-associated precipitation pattern.

The precipitation patterns associated with the  $\zeta_{850}$  and  $PV_{320}$  Pacific storm tracks reside equatorward of their respective mean intensity patterns. The peak precipitation rates are within the strongest gradients of the storm track's mean intensity pattern, not where the mean intensity patterns reach local maxima; the peak mean intensity of the  $\zeta_{850}$  and  $PV_{320}$  Pacific storm tracks reside northeast of the peaks in precipitation. In the  $PV_{320}$  pattern, a local peak in intensity resides over the western coast of North America between  $30^\circ\text{N}$  and  $60^\circ\text{N}$ , coinciding with the lysis density pattern of  $\zeta_{850}$ .

#### **4.3.2 North American-Atlantic Storm Track**

The precipitation pattern associated with the NAA storm track of  $\zeta_{850}$  resides equatorward of that storm track. The poleward gradient of this precipitation pattern lies within the  $\zeta_{850}$  NAA track. The precipitation peaks in the Gulf of Mexico and just east of the United States and resides equatorward of the  $\zeta_{850}$  NAA storm track.

The precipitation pattern associated with the NAA storm track of  $PV_{320}$  resides equatorward of that storm track. The poleward gradient of this precipitation pattern lies within the  $PV_{320}$  NAA track. The precipitation peaks east of Florida, USA and east of the United States and resides equatorward of the  $PV_{320}$  NAA storm track.

The precipitation patterns associated with the  $\zeta_{850}$  and  $PV_{320}$  NAA storm tracks reside equatorward of their respective mean intensity patterns. The peak precipitation rates

are within the strongest gradients of the storm track's mean intensity, not where the mean intensity patterns reach local maxima; the peak mean intensity of the  $\zeta_{850}$  and  $PV_{320}$  NAA storm tracks reside northeast of the  $\zeta_{850}$  and  $PV_{320}$  peaks in precipitation.

### 4.3.3 Mediterranean Storm Track

Like the  $PV_{320}$  Pacific and NAA precipitation patterns, the poleward  $PV_{320}$  Mediterranean precipitation gradient falls within its storm track, with the peak in precipitation rate just equatorward of the track. It is the equatorward Mediterranean precipitation gradient that lies within its respective storm track pattern, not the poleward precipitation gradient.

The peak mean intensity of the  $\zeta_{850}$  ( $PV_{320}$ ) Mediterranean storm track appears to reside just south (west) of its peak associated precipitation. This spatial relation is more easily seen in the  $PV_{320}$  pattern than the  $\zeta_{850}$  pattern as the magnitude of the peak Mediterranean precipitation of  $PV_{320}$  is about half of the corresponding Pacific and NAA precipitation peaks, whereas the  $\zeta_{850}$  Mediterranean precipitation is about one quarter of its corresponding Pacific and NAA peak magnitudes. In the Mediterranean Sea, it appears that the precipitation pattern follows the mean intensity's gradient east-southeast, though this is somewhat unclear.

## Chapter 5. Conclusions

Northern Hemisphere winter storm track dynamics are better depicted following the Lagrangian approach. Storm track spatial patterns, intensities, and characteristics are better defined using this method than those resulting from the traditional Eulerian method.

The Eulerian vorticity field emphasizes variability towards mid- and high-latitudes, underestimating the storm track strength in lower latitudes and overestimating the strength in high latitudes, especially above  $60^{\circ}\text{N}$  (as compared to the Lagrangian approach).

The use of the Lagrangian framework shows that isentropic potential vorticity is the preferred variable for diagnosing storm track patterns and behaviors.

When examining the effects of storm tracks on North American precipitation, the Lagrangian framework reveals that storm tracks characterized by isentropic potential vorticity leave a strong footprint on surface precipitation, especially over the Pacific and Atlantic Oceans. The precipitation pattern associated with cyclones derived from the IPV field shows small scale features of precipitation such as the enhanced precipitation signal over the western coast of North America due to orographic effects.

Future work will involve the investigation of the impacts of boreal winter storm tracks on extreme precipitation events over North America. We will examine to what extent hindcasts from the Climate Prediction Center's North American Multi-Model Ensemble (NMME) can reproduce the relationships between the Northern Hemisphere storm tracks and precipitation patterns over North America. We also plan to analyze the

effects of lower frequency modes of variability, such as the MJO and the North Atlantic Oscillation (NAO), on extreme precipitation events in North America. These studies will aid in the development of more accurate seasonal storm and precipitation forecasts, and they will further our understanding of the relationships between extreme precipitation events and storm tracks, and how lower frequency modes of variability play a role in these relationships.

## References

- Becker, E. J., E. H. Berbery, and R. W. Higgins, 2009: Understanding the characteristics of daily precipitation over the United States using the North American Regional Reanalysis. *J. Climate*, **22**, 6268-6286.
- Becker, E. J., E. H. Berbery, and R. W. Higgins, 2011: Modulation of cold-season U.S. daily precipitation by the Madden-Julian Oscillation. *J. Climate*, **24**, 5157-5166.
- Berbery, E. H., and C. S. Vera, 1996: Characteristics of the Southern Hemisphere winter storm track with filtered and unfiltered data. *J. Atmos. Sci.*, **53**, 468-481.
- Brayshaw, D. J., B. Hoskins, and M. Blackburn, 2008: The storm-track response to idealized SST perturbations in an aquaplanet GCM. *J. Atmos. Sci.*, **65**, 2842-2860.
- Chang, E. K. M., and I. Orlanski, 1993: On the dynamics of a storm track. *J. Atmos. Sci.*, **50**, 2038-2053.
- Chelliah, M., W. Ebisuzaki, S. Weaver, and A. Kumar, 2011: Evaluating the tropospheric variability in National Centers for Environmental Prediction's climate forecast system reanalysis. *J. Geophys. Res.*, **116**, D17107.
- Hawcroft, M. K., L. C. Shaffrey, K. I. Hodges, and H. F. Dacre, 2012: How much Northern Hemisphere precipitation is associated with extratropical cyclones? *Geophys. Res. Lett.*, **39**, L24809.
- Holton, J. R., 2004: An introduction to dynamical meteorology, Edition 4<sup>th</sup>. *Elsevier Academic Press*.
- Hoskins, B. J., and P. J. Valdes, 1990: On the existence of storm-tracks. *J. Atmos. Sci.*, **47**, 1854-1864.
- Hoskins, B. J., and T. Ambrizzi, 1993: Rossby wave propagation on a realistic longitudinally varying flow. *J. Atmos. Sci.*, **50**, 1661-1671.
- Hoskins, B. J., and K. I. Hodges, 2002: New perspectives on the Northern Hemisphere winter storm tracks. *J. Atmos. Sci.*, **59**, 1041-1061.
- Hsu, H.-H., and S.-H. Lin, 1992: Global teleconnections in the 250-mb streamfunction field during the Northern Hemisphere winter. *Mon. Wea. Rev.*, **120**, 1169-1190.
- Lu, R.-Y., J.-H. Oh, and B.-J. Kim, 2002: A teleconnection pattern in upper-level meridional wind over the North African and Eurasian continent in summer. *Tellus*, **54A**, 44-55.
- Orlanski, I., and E. K. M. Chang, 1993: Ageostrophic geopotential fluxes in downstream and upstream development of baroclinic waves. *J. Atmos. Sci.*, **50**, 212-225.
- Salathé, E. P., Jr., 2006: Influences of a shift in North Pacific storm tracks on western North American precipitation under global warming. *Geophys. Res. Lett.*, **33**, L19820.

- Trenberth, K. E., 1991: Storm tracks in the Southern Hemisphere. *J. Atmos. Sci.*, **48**, 2159-2178.
- Trenberth, K. E., A. Dai, R. M. Rasmussen, and D. B. Parsons, 2003: The changing character of precipitation. *BAMS*, **Sept. Edition**, 1205-1217.
- Wallace, J. M., G.-H. Lim, and M. L. Blackmon, 1988: Relationship between cyclone tracks, anticyclone tracks and baroclinic waveguides. *J. Atmos. Sci.*, **45**, 439-462.
- Wang, W., P. Xie, S. H. Yoo, Y. Xue, A. Kumar, and X. Wu (2011), An assessment of the surface climate in the NCEP climate forecast system reanalysis, *Clim. Dyn.*, in press.